Turkish Journal of Electrical Engineering & Computer Sciences

http://journals.tubitak.gov.tr/elektrik/

Research Article

Turk J Elec Eng & Comp Sci
(2015) 23: 1645 – 1659

doi:10.3906/elk-1404-275

Variable charge/discharge time-interval control strategy of BESS for wind power dispatch

Wei CHAI*, **Zheng LI**, **Xu CAI**
Wind Power Research Center, School of Electronic Information and Electrical Engineering,
Shanghai Jiao Tong University, Shanghai, P.R. China

Received: 14.04.2014 • **Accepted/Published Online:** 27.12.2014 • **Printed:** 30.11.2015

Abstract: A variable charge/discharge time-interval ($T_{C/D}$) control strategy of a battery energy storage system (BESS) for wind power dispatch is proposed in this paper, aiming at: 1) extending the BESS life, 2) reducing the total BESS energy loss, and 3) increasing the dispatch tracking accuracy. A multifactor life model of a large-scale BESS containing four factors, charge/discharge rate, times, $T_{C/D}$, and temperature, is developed, which has taken into account the cell series/parallel effects and BESS operational characteristics. A comprehensive evaluation system including BESS aging level (BAL), energy loss index (ELI), and tracking inaccuracy index (TII) is proposed, and the relationships between $T_{C/D}$ and the three indices are discussed. In order to combine the advantages of low BAL and low ELI under long $T_{C/D}$ and low TII under short $T_{C/D}$, a fuzzy controller is designed to regulate $T_{C/D}$ in real time. The effectiveness of the proposed control strategy is verified by actual data from a wind farm in eastern China.

Key words: Battery energy storage system, wind power dispatch, battery life, storage energy loss, fuzzy control

1. Introduction

Wind energy is considered to be one of the most promising renewable energy sources. However, wind farms are difficult to be dispatched like conventional thermal power plants because of the fluctuant and intermittent output power. Moreover, the high wind penetration level and the unbalance between supply and load will adversely impact the stability of the system. Instead of maximum power point tracking, wind power has to be curtailed for system security, in which case much energy is wasted [1].

The idea of applying a battery energy storage system (BESS) to mitigate fluctuation and intermittency of wind power has attracted much attention [2–4]. Unfortunately, the limited battery life, the charge/discharge energy loss, and the high installation cost restrict the application of BESS. Current studies mostly focus on how to use BESS economically and effectively. In [5], for example, a method of planning and operating BESS for wind power dispatch was presented. The authors carried out an economic analysis to address the feasibility and profitability of the wind/storage system. In [6], a model predictive control scheme of energy storage was proposed to solve the power deviations and to optimize the system economic revenue. However, these studies chose the BESS life-year as a default value from experience rather than estimating BESS life based on theoretical derivation considering the actual running conditions.

In most studies, the main control target of the BESS is to improve the grid-connection performance,

*Correspondence: chaiweisjtu@sjtu.edu.cn

rather than reducing the BESS aging level or its charge/discharge energy loss [7–14]. For instance, a two-time-scale control approach for BESS was developed in [7,8] to smooth the wind power. In [9,10], the BESS was controlled to make the wind power more dispatchable. In [11], an application of BESS was presented in order to mitigate wind power variation, improve wind energy integration, and enhance voltage stability. As for protection of the BESS, only several simple constraints have been taken into account, such as the current limitation [12,13] and the state-of-charge (SOC) limitation [14,15]

Few research studies have addressed the control methods that postpone BESS aging effects considering the variable load and complicated environment. To this end, a BESS life model needs to be developed. Meanwhile, the life model can also be used to evaluate BESS control effects. Extended efforts have been made to develop the battery life model [16–21], but few studies referred to large-scale BESS for fluctuant power applications. A semiempirical life model for lithium ion cells was established based on a significant amount of experimental data in [16]. In [17], the authors proposed a partially linearized life model for electric vehicle batteries. Unlike a single cell or electric vehicle batteries, the storage capacity needed for wind power dispatch is very large, and so it is hard to conduct enough experiments to test the BESS life under different conditions. In [18], a life model of BESS in microgrid applications was developed by applying Peukert's law for depth of discharge (DOD) and cycle times. However, this model neglects the various charge/discharge rates and the series/parallel patterns that affect BESS life.

This paper proposes a variable charge/discharge time-interval ($T_{C/D}$) control strategy of BESS for wind power dispatch. The objectives of this control strategy are: 1) increasing the dispatch tracking accuracy, 2) extending the BESS life, and 3) reducing the BESS energy loss. To this end, 3 evaluation indices including tracking inaccuracy index (TII), BESS aging level (BAL), and energy loss index (ELI) are defined. A multifactor life model of the BESS containing four factors, charge/discharge rate, times, $T_{C/D}$, and temperature, is developed, which has taken into account the cell series/parallel effects and the characteristics of the BESS for wind power dispatch. After discussing the relationships between $T_{C/D}$ and the 3 indices, we design a fuzzy controller to regulate $T_{C/D}$ in real time in order to solve the problems of short BESS life and high energy loss under short $T_{C/D}$ and low tracking accuracy under long $T_{C/D}$. The effectiveness of the proposed control strategy is verified by actual data from a wind farm in eastern China.

2. Evaluation indices of BESS for wind power dispatch

2.1. BESS control modes and the tracking inaccuracy index

Wind farms are difficult to be dispatched like conventional thermal power plants because of the fluctuant and intermittent output power, which will adversely impact the stability and reliability of the system. Therefore, there is a need for dispatching the wind energy based on a reference power profile. This reference power profile is the dispatch order P_{ref}. P_{ref} can be set as the average wind power output P_{avg} during the dispatch period T_d:

$$P_{ref} = \alpha \cdot P_{avg} \quad (\alpha < 1), \tag{1}$$

where α is a charge/discharge balance coefficient considering BESS energy loss. The BESS can be controlled to compensate the difference between P_{ref} and the wind power output P_{wind}, so that the total power injected to the grid can track P_{ref} more accurately. Thus, the BESS output power P_b is ($P_b > 0$ when discharge, $P_b <$

0 when charge):

$$P_b = \begin{cases} (\alpha P_{avg} - P_{wind})/\eta_d, P_{ref} > P_{wind} \\ \alpha P_{avg} - P_{wind}, P_{ref} \le P_{wind} \end{cases}, \quad (2)$$

where η_d is the BESS discharge efficiency. Moreover, the SOC of the BESS should be restricted in ($\mathrm{SOC}_{\min}$, $\mathrm{SOC}_{\max}$). $P_{bmax,ch}$ denotes the maximum allowable charge power of the BESS, and $P_{bmax,dsc}$ represents the maximum allowable discharge power. The rated capacity, the charge efficiency, and the voltage of BESS are C_{rated}, η_d, and u_b, respectively. Therefore, P_b should comply with the following constraints:

$$\begin{cases} P_b \ge (\mathrm{SOC} - \mathrm{SOC}_{\max}) C_{rated} u_b / (T_{C/D} \eta_c), P_{ref} \le P_{wind} \\ P_b \le (\mathrm{SOC} - \mathrm{SOC}_{\min}) C_{rated} u_b / T_{C/D}, P_{ref} > P_{wind} \\ P_{b\max,ch} \le P_b \le P_{b\max,dsc} \end{cases}. \quad (3)$$

$T_{C/D}$ is the BESS charge/discharge time-interval, which is the duration of each control operation of BESS, i.e. the duration of P_b. Because of the BESS constraints and the wind power variability, the combined output of the wind farm and the BESS does not always track P_{ref} accurately. Hence, the question is how to control the BESS to improve the dispatch tracking accuracy. There are 2 BESS control modes according to the way $T_{C/D}$ is determined:

1) Fixed $T_{C/D}$ control (FTC) mode: in this mode, every charge/discharge operation of the BESS lasts the same amount of time. The impacts of $T_{C/D}$ on BESS control effects are discussed in Section 3.1. The dispatch tracking accuracy will be higher when the $T_{C/D}$ is shorter, but the high frequency of charge/discharge will have an adverse effect on BESS aging level and energy loss, and so it is important to make a good choice of $T_{C/D}$.

2) Variable $T_{C/D}$ control (VTC) mode: in this mode, the duration of the BESS control window is changing in real time so as to improve the dispatch tracking accuracy, at the same time decreasing the BESS aging level and energy loss.

TII is defined to represent the tracking performance of the total power injected to the grid P_{grid}, which shows the control effect of the BESS for wind power dispatch.

$$P_{grid} = P_b + P_{wind} \quad (4)$$

If the sampling period of wind power is T_s and the initial time is t_0, then the TII of the ith sampling period TII_i can be defined as follows:

$$TII_i = \frac{|P_{grid}(t_0 + iT_s) - P_{ref}(t_0 + iT_s)|}{P_{ref}(t_0 + iT_s)} \times 100\%. \quad (5)$$

From the above equation, it is obvious that a smaller TII indicates higher dispatch tracking accuracy. Therefore, if TII is small, risks of reliability, stability, and economic penalties and energy wasted will be reduced.

2.2. The index of the BESS aging level (BAL)

The lithium ion battery is one of the most widely used storage batteries in large-scale applications. From the view of electrochemistry, the formation of the solid electrolyte interphase should be responsible for the battery aging, which leads to capacity fade and impedance rise [19]. From the external characteristics, there are a variety of factors that influence battery aging, such as charge/discharge rate, DOD, and temperature.

2.2.1. Ah-throughput life model

"Cycle life" is often used to describe the life of the BESS, which is the total number of cycles before batteries reach the end of life (EOL) under standard test conditions when fully charged and discharged at a constant rate. However, in wind power dispatch applications, the BESS is not charged or discharged at regular and repeating intervals. In this case, the BAL is mainly associated with its Ah-throughput, which is the total quantity of charge throughout the BESS life [20].

The rated capacity C_{rated}(Ah) and cycle life N (cycles) of the BESS are given by the manufacturer. A complete full cycle consists of two parts: a complete half cycle of charge and a complete half cycle of discharge. The Ah-throughput of each complete half cycle is C_{rated}. Therefore, the total expected Ah-throughput C before EOL is supposed to be:

$$C = 2N \cdot C_{rated}. \tag{6}$$

The BESS is charged or discharged based on the power and time instructions given by the BESS controller. For example, the kth power-instruction P_b^k is the kth charge/discharge output power of BESS, and the kth time-instruction $T_{C/D}^k$ is the kth charge/discharge time-interval as well as the duration of P_b^k. Thereby, the kth Ah-throughput C^k is:

$$C^k = \frac{\left|P_b^k\right| \cdot T_{C/D}^k}{u_b^k}, \tag{7}$$

where u_b^k is the BESS voltage of the kth charge/discharge. In the Ah-throughput life model, the BESS aging level BAL_{Ah} is defined as follows:

$$BAL_{Ah} = \sum_{k=1}^{K} \frac{C^k}{C} \times 100\% \ , \tag{8}$$

where K is the charge/discharge times, or the number of half cycles. $BAL_{Ah} = 0$ represents that the BESS is completely new, and $BAL_{Ah} = 1$ represents that the BESS has reached its EOL.

The Ah-throughput life model is a simple linear model that can be easily calculated and applied, but it neglects the factors that affect BESS life such as the variable charge/discharge rate, DOD, and temperature.

2.2.2. Multifactor life model

Capacity fade is an important characteristic that can show the BESS aging level. Based on the factors of charge/discharge rate, cycle times, DOD, and temperature, the capacity fading rate of a single lithium ion cell f_{Si} can be expressed as follows [16]:

$$f_{Si} = B_i \exp\left(\frac{-a_1 + a_2 C_i}{RT}\right) \cdot (2M \cdot \mathrm{DOD})^z, i = 1, 2, 3, 4, \tag{9}$$

where T is the absolute temperature, M is the number of cycles, R is the gas constant, C_i is the charge/discharge rate ($C_1 = 0.5$, $C_2 = 2$, $C_3 = 6$, $C_4 = 10$), and B_i is a coefficient with different C_i. The parameters of B_i, a_1, a_2, and z can be fitted based on experimental data. If the simulation results of f_{Si} under various conditions are in general agreement with the experimental data, the parameters of the above equation are reliable [16].

The BESS is composed of numerous cells in series and parallel to enlarge its capacity. The cells are connected in parallel to get more current and connected in series to boost output voltage. This series/parallel

pattern is designed to make every cell share the total Ah-throughput of the BESS equally. However, the great number of cells connected in series and parallel can easily lead to unbalance in voltages and currents among the cells and form circulation currents, which will have an adverse effect on BESS life. Therefore, the capacity fading rate of large-scale BESS f_{Li} can be deduced from Eq. (9) as:

$$f_{Li} = B_i \exp\left(\frac{-a_1 + a_2 C_i}{RT}\right) \cdot \left(\frac{N_S C_{rated,S}}{N_L C_{rated,L}} 2M \times \mathrm{DOD}\right)^z, i = 1, 2, 3, 4, \tag{10}$$

where N_S and $C_{rated,\,S}$ are the cycle life and rated capacity of a single cell, and N_L and $C_{rated,\,L}$ are the cycle life and rated capacity of large scale BESS. The cycle life of a large-scale BESS is much smaller than a single cell because of the series/parallel pattern, so in Eq. (10), N_S / N_L represents the intensified aging effect resulting from unbalanced voltages and currents. In addition, $C_{rate,\,S}$ / $C_{rate,\,L}$ represents every single cell sharing BESS total Ah-throughput equally.

The output power of the BESS for wind power dispatch is fluctuant irregularly due to the randomness of wind energy. Thus, the charge/discharge rate and time-interval of the BESS are various in every half cycle, but the life model of Eq. (10) is only suitable for the cycle mode in which $2M \times \mathrm{DOD}$ means the total Ah-throughput. For wind power dispatch, the total Ah-throughput of the BESS can be described as:

$$Ah_i = \begin{cases} \sum_{k=1}^{K} \frac{|P_b^k| \cdot T_{C/D}^k}{u_b^k}, 0 < \frac{|P_b^k|}{u_b^k I_{1C}} \le 0.5, i = 1 \\ \sum_{k=1}^{K} \frac{|P_b^k| \cdot T_{C/D}^k}{u_b^k}, 0.5 < \frac{|P_b^k|}{u_b^k I_{1C}} \le 2, i = 2 \\ \sum_{k=1}^{K} \frac{|P_b^k| \cdot T_{C/D}^k}{u_b^k}, 2 < \frac{|P_b^k|}{u_b^k I_{1C}} \le 6, i = 3 \end{cases}, \tag{11}$$

where Ah_i is the total accumulated Ah-throughput of the BESS under different charge/discharge rates, and I_{1C} is the rated current corresponding to 1 charge/discharge rate. A high charge/discharge rate is forbidden for the protection of the BESS, so a charge/discharge rate over 6 is not taken into account. Combining Eqs. (10) and (11), in a multifactor life model the BESS aging level BAL_{mf} is defined as:

$$BAL_{mf} = \sum_{i=1}^{3} \left[B_i \exp\left(\frac{-a_1 + a_2 C_i}{RT}\right) \cdot \left(\frac{N_S C_{rate,S}}{N_L C_{rate,L}} \cdot Ah_i\right)^z \right] \times 100\%. \tag{12}$$

The multifactor life model of the BESS deduced from the capacity fading rate of a single cell has taken into account the factors of charge/discharge rate, charge/discharge times, $T_{C/D}$, and temperature, as well as the characteristics of a large-scale BESS for wind power dispatch. Therefore, it can be used to optimize the control strategy of the BESS and evaluate the control effect on BAL.

2.3. The energy loss index

The charge efficiency η_c and discharge efficiency η_d of the BESS are provided by the manufacturers, so the BESS energy loss of each charge/discharge control operation EL^k can be described as:

$$EL^k = \begin{cases} (1 - \eta_c) \times (-P_b^k) T_{C/D}^k, P_b^k \le 0 \\ (1 - \eta_d) \times P_b^k T_{C/D}^k, P_b^k > 0 \end{cases}. \tag{13}$$

ELI represents the total energy loss of the BESS normalized by the electricity production of the wind farm, which is the integral of P_{wind} times the corresponding time t:

$$ELI = \frac{1}{\int_t P_{wind} t} \sum_{k=1}^{K} EL^k \times 100\% \ . \tag{14}$$

3. Variable $T_{C/D}$ control strategy of BESS for wind power dispatch

3.1. Relationships between $T_{C/D}$ and the three indices

Since P_{wind} is changing all the time while P_b remains the same during the period of $T_{C/D}$, the length of $T_{C/D}$ has an impact on the tracking accuracy of wind power dispatch. The relationships between TII and $T_{C/D}$ under different dispatch periods (T_d) are shown in Figure 1 in the case that the BESS is controlled for wind power dispatch in the FTC mode as mentioned in Section 2.1 and running continuously for 1 year. In addition, the configuration of the wind/BESS farm is presented in Section 4.1. It can be seen that the longer T_d is, the higher TII will be, because the BESS will need more capacity and higher power to compensate the difference between P_{wind} and P_{ref} when T_d is longer, and the limitations of SOC and P_b result in the decrease of dispatch tracking accuracy. However, no matter how long T_d is, the dispatch tracking accuracy will be higher when $T_{C/D}$ is shorter.

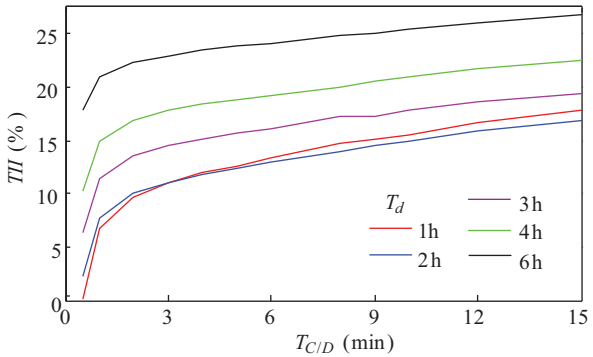

Figure 1. Relationships between TII and $T_{C/D}$ under different T_ds.

BAL_{Ah} and BAL_{mf} corresponding to different $T_{C/D}$s are represented in Figure 2, in which case the BESS is also controlled in FTC mode and running for 1 year. It can be seen that when T_d is 1 h, BESS life conditions are the best, because when T_d is shorter, the charge/discharge rate and the total accumulated Ah-throughput needed are smaller. However, a longer T_d will lead to deficiency of BESS capacity and the BESS will stop charge or discharge due to the SOC constraint. Consequently, the BESS aging process will be slowed down when T_d is too long, which is why BAL of T_d = 6 h is better than that of 2 h. Regardless of T_d, the longer $T_{C/D}$ is, the lower BAL_{Ah} and BAL_{mf} will be, because the high frequency of charge/discharge will have an adverse effect on BAL.

The relationships between ELI and $T_{C/D}$ under different T_ds are shown in Figure 3 when the BESS is also controlled in FTC mode and running for 1 year. As seen, with the extending of $T_{C/D}$, ELI is reduced slightly. Thus, the longer $T_{C/D}$ shows a better performance in terms of ELI.

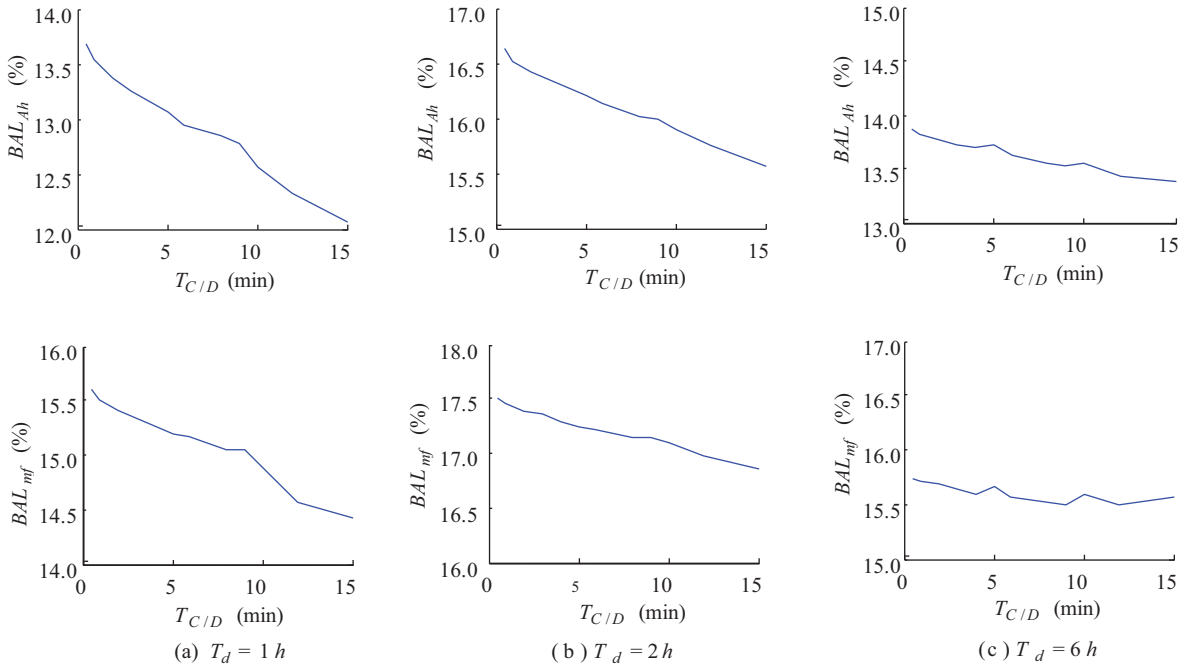

Figure 2. Relationships between BAL and $T_{C/D}$ under different T_ds.

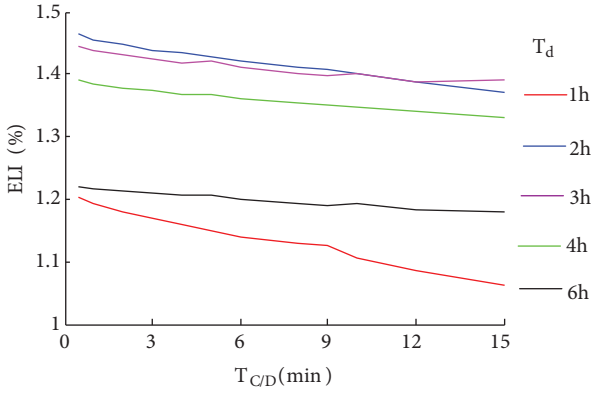

Figure 3. Relationships between ELI and $T_{C/D}$ under different T_ds.

As mentioned above, the BESS is controlled based on the power instruction P_b^k and the corresponding time instruction $T_{C/D}^k$. The BESS capacity fading rate BAL_{mf}^k and energy loss EL^k of a single charge/discharge operation, which can also be seen as a half cycle, is calculated in Figure 4 when the BESS is charged/discharged with the output power of P_b^k for the time-interval of $T_{C/D}^k$. It is evident that with the rise of P_b^k, BAL_{mf}^k and EL^k are both increased since the charge/discharge rate is higher and the Ah-throughput of this half cycle is larger. With the same P_b^k, the longer $T_{C/D}^k$ is, the higher BAL_{mf}^k and EL^k are, since Ah-throughput during the longer $T_{C/D}^k$ is larger.

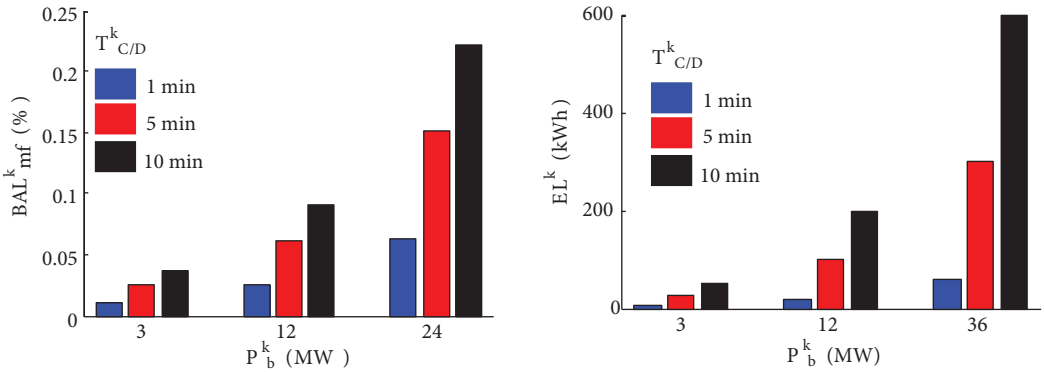

Figure 4. BAL^k_{mf} (left) and EL^k (right) of a half cycle with different P^k_bs and $T^k_{C/D}$s.

3.2. Design of variable $T_{C/D}$ fuzzy controller

The objectives of the proposed control strategy are: 1) extending the BESS life, 2) improving the BESS energy efficiency, and 3) increasing the dispatch tracking accuracy. It was illustrated that $T_{C/D}$ has impacts on BAL, ELI, and TII in certain patterns in Section 3.1, and so we come up with the idea of variable $T_{C/D}$ control. The time interval of each charge/discharge operation $T^k_{C/D}$ is chosen in real time in order to achieve the above three objectives. The main principles of the determination of $T^k_{C/D}$ are proposed based on relationships between $T_{C/D}$ and the three indices as follows:

a) When the BESS power instruction P^k_b is high, a shorter $T^k_{C/D}$ should be chosen. Because the higher P^k_b has an adverse effect on BAL and ELI, a shorter $T^k_{C/D}$ can shorten the duration of this adverse effect and reduce Ah-throughput so as to extend the BESS life and improve the BESS energy efficiency.

b) Accordingly, a longer $T^k_{C/D}$ should be chosen when P^k_b is low.

c) When the dispatch tracking inaccuracy at the present TII^k is high, the quality of P_{grid} should be considered first. In this case, a shorter $T^k_{C/D}$ should be chosen, yet a longer $T^k_{C/D}$ is forbidden for the good of TII.

d) When TII^k is low, which means that the performance of P_{grid} meets the requirement, $T^k_{C/D}$ should be chosen based on P^k_b as mentioned in principles (a) and (b) for the good of BAL and ELI.

In order to regulate $T^k_{C/D}$ in real time, a fuzzy controller is designed based on the principles above. Membership functions of the output and inputs are shown in Figure 5. The output of the fuzzy controller is$T^k_{C/D}$ in a discrete domain (universe of discourse): $T^k_{C/D} \in \{0.5, 1, 1.5, 2 \ldots 14.5, 15\}$ (min). The linguistic terms of $T^k_{C/D}$ are defined as {ZE, VS, MS, ML, VL} and their membership functions e_{TCD} are presented in Figure 5a. There are 2 inputs, P^k_b and TII^k, in this fuzzy controller. The universe of discourse of input P^k_b is a finite continuous domain, $P^k_b \in$ [-24, 24] (MW), and the linguistic terms are {NH, NL, ZE, PL, PH} with the membership functions e_P presented in Figure 5b. The other input TII^k is in an infinite continuous domain,

$TII^k \in [0, +\infty)$ (%), and the linguistic terms are {ZE, VL, ML, MH, VH} with the membership functions e_{TII} presented in Figure 5c. The rules of this 2-inputs, 1-output fuzzy controller are shown in Table 1 based on the aforementioned 4 principles.

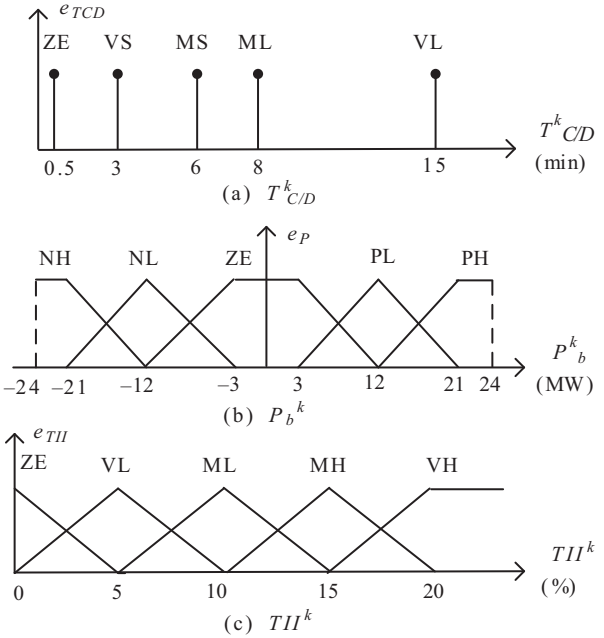

Figure 5. Membership functions of the output and inputs.

Table 1. Fuzzy control rules.

TII^k	P_b^k				
	NH	NL	ZE	PL	PH
ZE	ZE	VL	VL	VL	ZE
VL	ZE	ML	VL	ML	ZE
ML	ZE	MS	ML	MS	ZE
MH	ZE	VS	MS	VS	ZE
VH	ZE	ZE	ZE	ZE	ZE

The defuzzification algorithm of the center of gravity [22] is employed to obtain the defuzzified output value$T_{C/D}^k$, and it should be rounded due to the discrete domain:

$$T_{C/D}^k = \frac{1}{2}\text{round}(2 \times \frac{\sum_{x=1}^{5}\sum_{y=1}^{5} e_{TII,x}(TII^k)e_{P,y}(P_b^k)T_{C/D,x,y}^k}{\sum_{x=1}^{5}\sum_{y=1}^{5} e_{TII,x}(TII^k)e_{P,y}(P_b^k)}), \tag{15}$$

where round (•) is the rounding function, x is the index of linguistic terms of input TII_k, and y is the index of linguistic terms of input P_b^k.

4. Case study

4.1. Configuration of the studied system

A 60-MW wind farm in eastern China is employed in this study. It is equipped with a 6-MWh lithium ion BESS. The configuration of the BESS is shown in Table 2.

Table 2. The configuration of BESS.

SOCmin	SOCmax	SOC(0)	$P_{bmax,dsc}$	$P_{bmax,ch}$	η_c	η_d	α
10%	90%	45%	24 MW	–24 MW	0.9	0.9	0.895

The 6-MWh BESS is composed of numerous 2.2-Ah cells in series and parallel. The cycle life of a single cell is 10,000 cycles, its largest charge rate is 6, and the largest discharge rate is 10. After the cells are connected in series and parallel, the cycle life of the large-scale BESS is 6000 cycles and the largest charge/discharge rate is 4. Since a ventilation cooling system is equipped in the BESS, the temperature is supposed to be 25 °C constantly. Some other parameters of the BESS life model are presented in Table 3.

Table 3. Parameters of BESS life model.

B_1	B_2	B_3	a_1	a_2	R	z
31,630	21,681	12,934	31,700	370.3	8.314	0.55

4.2. Simulation results of the variable $T_{C/D}$ control strategy

Performance of the wind/BESS farm applied with the proposed fuzzy VTC strategy from 1700 hours on 24 October 2012 to 0800 hours the next day is presented in Figure 6. In comparison, performance of the FTC method for $T_{C/D}$ of 4 min is also given in Figure 6. The sampling period T_S is 30 s, and the dispatch period T_d is 2 hours. Figure 6a shows that with the help of the BESS, the P_{grid} of both strategies can track P_{ref} very well, and the wind farm can be more dispatchable accordingly. The details during A1–A3 are magnified to be more clearly seen in Figure 6b. It is obvious that the $T_{C/D}$ of the FTC strategy is 4 min constantly. However, the $T_{C/D}$ of the VTC strategy varies based on the fuzzy control rules. For example, $|P_b|$ of A3 is very low and P_{grid} tracks P_{ref} with great accuracy in A3; therefore, a longest $T_{C/D}$ of 15 min is chosen based on the fuzzy rules. As for A2, $|P_b|$ is higher, but the tracking accuracy is also high, and therefore the $T_{C/D}$ of A2 is just a little shorter than that of A3. In A1, $|P_b|$ is relatively high, while the tracking accuracy is low, and thus a shorter $T_{C/D}$ of 8 min is chosen to reduce the TII of A1. It can be seen from Figure 6c that $T_{C/D}$, the duration of each P_b, is changing in real time in the VTC mode, while the $T_{C/D}$ of the FTC mode remains the same. Figure 6d indicates that the SOC of both strategies are within the limitations all the time.

The probability distribution of $T_{C/D}$ is shown in Figure 7 based on the sample data of the wind/BESS farm applied with the VTC strategy in 2012. It is obvious that the probability is higher when $T_{C/D}$ is 0.5 min, 6–8 min, and 15 min because of the design of $T^k_{C/D}$ membership functions and the fuzzy control rules. Since the number of rules where $T^k_{C/D}$ is ZE is the largest, the probability of $T^k_{C/D}$ to be 0.5 min is the highest, which is up to 51%. Furthermore, the probability of $T^k_{C/D}$ to be 15 min is also very high at a percentage of 29%, because the situation that $|P_b| < 3$ MW and $TII < 10\%$ is very common.

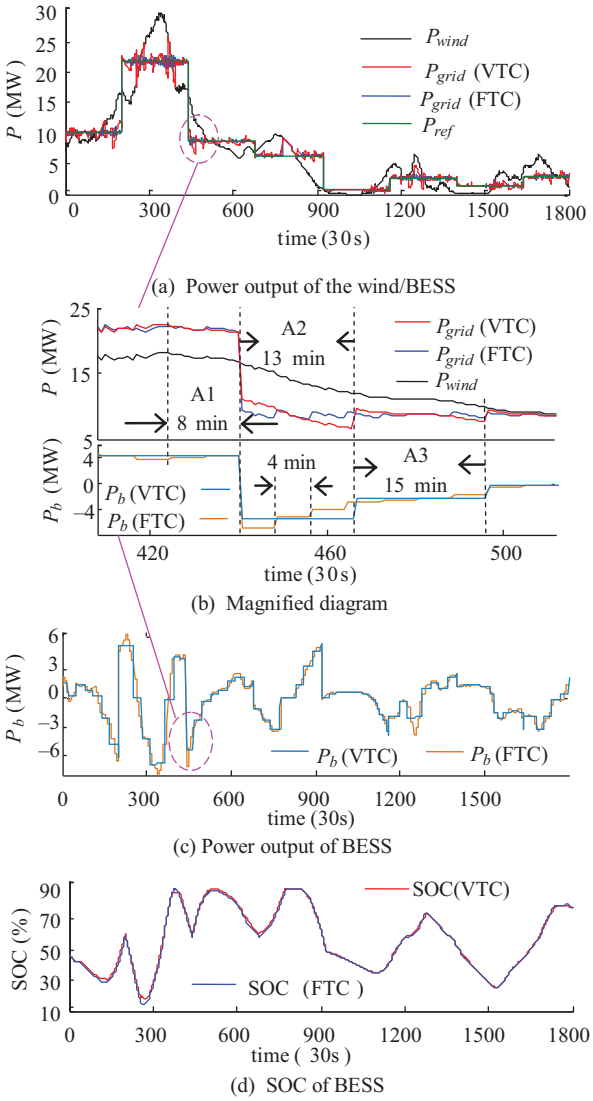

Figure 6. Performance of the wind/BESS farm applied with the VTC strategy.

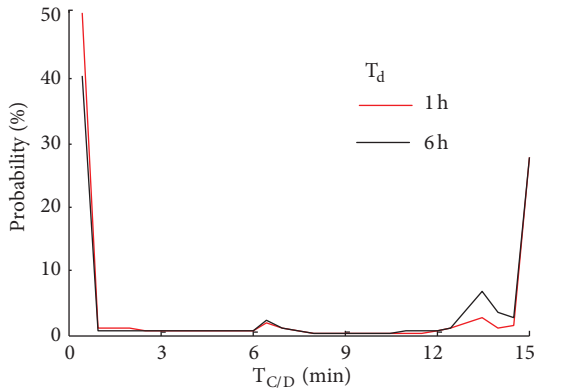

Figure 7. Probability distribution of $T_{C/D}$ in the VTC mode.

4.3. Comparisons between the fixed $T_{C/D}$ control and variable $T_{C/D}$ control

Comparisons between FTC and VTC in TII, BAL, and ELI are shown in Tables 4–6 when the wind/BESS farm is running for 1 year with T_d of 1 h, 2 h, and 6 h, respectively. Eight $T_{C/D}$s among 0.5–15 min are selected in the FTC mode and the proposed fuzzy controller is applied in the VTC mode. It can be seen from the tables that the proposed fuzzy VTC strategy has combined the advantages of long BESS life and low energy loss when $T_{C/D}$ is long and high tracking accuracy when $T_{C/D}$ is short. As shown in the tables, TII of VTC is equal to that of a short $T_{C/D}$ (i.e. 4–6 min) in FTC mode, yet BAL and ELI of VTC are equal to that of a long $T_{C/D}$ (i.e. 12–15 min) in FTC mode, and thus the three indices are all optimized no matter how long T_d is.

Table 4. Comparisons between FTC mode and VTC mode (T_d = 1 h).

FTC mode									VTC mode
$T_{C/D}$ (min)	0.5	2	4	6	8	10	12	15	
TII (%)	0.19	9.74	11.91	13.27	14.70	15.57	16.69	17.92	12.59
BAL_{Ah} (%)	13.67	13.37	13.15	12.95	12.84	12.57	12.32	12.06	12.21
BAL_{mf} (%)	15.63	15.44	15.28	15.19	15.06	14.89	14.58	14.43	14.58
ELI (%)	1.2	1.18	1.16	1.14	1.13	1.11	1.09	1.06	1.08

Table 5. Comparisons between FTC mode and VTC mode (T_d = 2 h).

FTC mode									VTC mode
$T_{C/D}$ (min)	0.5	2	4	6	8	10	12	15	
TII (%)	2.29	10.06	11.82	13.00	13.96	14.94	15.90	16.93	12.53
BAL_{Ah} (%)	16.62	16.42	16.27	16.14	16.00	15.89	15.75	15.56	15.64
BAL_{mf}(%)	17.54	17.43	17.33	17.25	17.17	17.12	17.02	16.90	16.96
ELI (%)	1.46	1.45	1.43	1.42	1.41	1.40	1.39	1.37	1.38

Table 6. Comparisons between FTC mode and VTC mode (T_d = 6 h).

FTC mode									VTC mode
$T_{C/D}$ (min)	0.5	2	4	6	8	10	12	15	
TII (%)	17.77	22.36	23.41	24.08	24.78	25.47	26.02	26.75	23.69
BAL_{Ah} (%)	13.86	13.78	13.70	13.62	13.55	13.55	13.43	13.38	13.39
BAL_{mf} (%)	15.77	15.72	15.62	15.60	15.56	15.63	15.53	15.60	15.55
ELI (%)	1.22	1.21	1.21	1.20	1.19	1.19	1.18	1.18	1.18

Durable years of BESS applied with different control modes are presented in Figure 8, which are calculated based on the data of the wind/BESS farm in 2012. The horizontal axis represents $T_{C/D}$ of FTC modes and the symbol '+' represents BESS durable years in VTC mode applied with the proposed fuzzy controller. In the Ah-throughput life model, the BESS reaches EOL when BAL_{Ah} is up to 100%, as shown in Figure 8a, and in Figure 8b, BAL_{mf} in the multifactor life model is considered to be 40% when the BESS reaches the EOL. Comparing the two figures, durable years of the multifactor life model are shorter than that of the Ah-throughput life model, but the variation tendencies of the two life models in different control modes are almost the same. The wind powers dispatched with different T_ds are shown respectively, and it can be seen that no matter how long T_d is, the durable years of BESS in VTC mode are equal to that of a long $T_{C/D}$ (i.e. 12–15 min) in FTC mode; thus, the BESS life has been extended by means of the proposed VTC strategy.

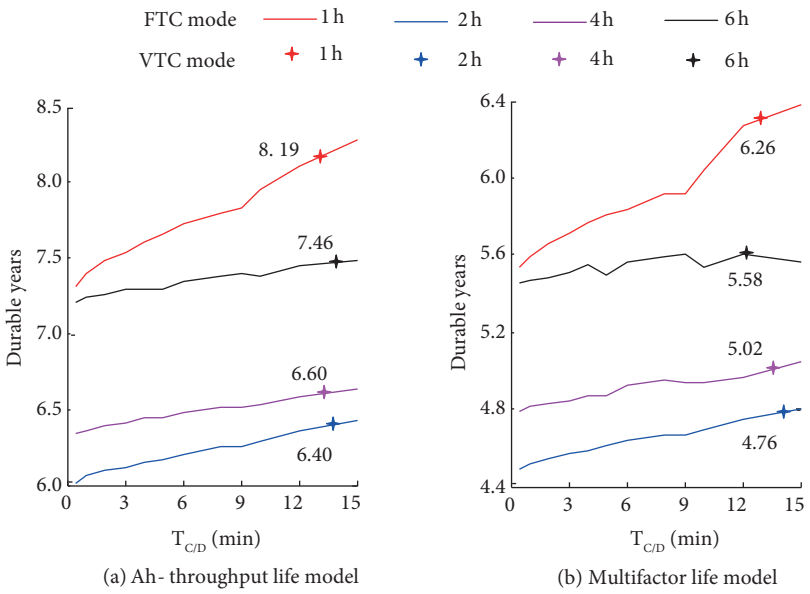

Figure 8. Durable years of BESS applied with different control modes.

Probability distributions of TII_j in different control modes are shown in Figure 9. It is obvious that the probability that $TII_j < 10\%$ is very high, which means that P_{grid} can track P_{ref} accurately most of the time. The probability that $TII_j < 10\%$ in VTC mode is improved slightly compared with that of $T_{C/D}$ being 15 min in FTC mode. Meanwhile, the probability that $TII_j > 30\%$ in VTC mode is very low, almost equal to that of $T_{C/D}$ being 2 min in FTC mode.

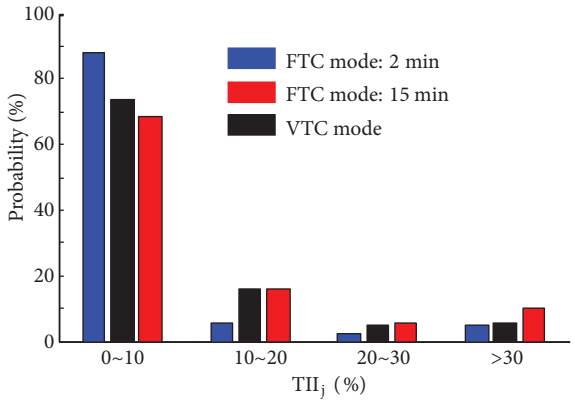

Figure 9. Probability distributions of TII_j in different control modes.

5. Conclusion

In this paper, three indices of BESS (TII, BAL, and ELI) are defined for wind power dispatch, and the relationships between $T_{C/D}$ and the three indices are discussed, based on which a fuzzy variable $T_{C/D}$ controller is designed. According to the results of the case study, we can come to following conclusions: 1) The BESS can improve the dispatch tracking accuracy of the wind power. Meanwhile, the shorter the $T_{C/D}$ is, the lower the TII will be. 2) BAL_{mf} from the proposed multifactor life model of BESS is a little higher than BAL_{Ah} from

the Ah-throughput life model, but their variation tendencies in different control modes are almost the same. 3) The longer the $T_{C/D}$ is, the lower BAL and ELI will be. 4) The length of T_d can affect the performance of the BESS. 5) No matter how long T_d is, TII of VTC is equal to that of a short $T_{C/D}$ (4–6 min) in FTC mode, and BAL and ELI of VTC are equal to that of a long $T_{C/D}$ (12–15 min). Therefore, the proposed fuzzy VTC strategy has combined the advantages of long BESS life and low energy loss under long $T_{C/D}$ and high tracking accuracy under short $T_{C/D}$.

Acknowledgment

This research was supported by the National High Technology Research and Development Program of China (863 Program), 2012AA050203.

References

[1] Ling Y, Cai X. Exploitation and utilization of the wind power and its perspective in China. Renew Sust Energ Rev 2012; 16: 2111–2117.

[2] Wee KW, Choi SS, Vilathgamuwa DM. Design of a least-cost battery-supercapacitor energy storage system for realizing dispatchable wind power. IEEE T Sustain Energ 2013; 4: 786–796.

[3] Gyawali N, Ohsawa Y, Yamamoto O. Power management of double-fed induction generator-based wind power system with integrated smart energy storage having superconducting magnetic energy storage/fuel-cell/electrolyser. IET Renew Power Gen 2011; 5: 407–421.

[4] Goel PK, Singh B, Murthy SS, Kishore N. Isolated wind-hydro hybrid system using cage generators and battery storage. IEEE T Ind Electron 2011; 58: 1141–1153.

[5] Dicorato M, Forte G, Pisani M, Trovato M. Planning and operating combined wind-storage system in electricity market. IEEE T Sustain Energ 2012; 3: 209–217.

[6] Perez E, Beltran H, Aparicio N, Rodriguez P. Predictive power control for PV plants with energy storage. IEEE T Sustain Energ 2013; 4: 482–490.

[7] Jiang Q, Haijiao W. Two-time-scale coordination control for a battery energy storage system to mitigate wind power fluctuations. IEEE T Energy Conver 2013; 28: 52–61.

[8] Jiang Q, Hong H. Wavelet-based capacity configuration and coordinated control of hybrid energy storage system for smoothing out wind power fluctuations. IEEE T Power Syst 2013; 28: 1363–1372.

[9] Teleke S, Baran M E, Bhattacharya S, Huang A Q. Rule-based control of battery energy storage for dispatching intermittent renewable sources. IEEE T Sustain Energ 2010; 1: 117–124.

[10] Teleke S, Baran ME, Bhattacharya S, Huang AQ. Optimal control of battery energy storage for wind farm dispatching. IEEE T Energy Conver 2010; 25: 787–794.

[11] Le HT, Santoso S, Nguyen TQ. Augmenting wind power penetration and grid voltage stability limits using ESS: application design, sizing, and a case study. IEEE T Power Syst 2012; 27: 161–171.

[12] Wang P, Gao Z, Bertling L. Operational adequacy studies of power systems with wind farms and energy storages. IEEE T Power Syst 2012; 27: 2377–2384.

[13] Gabash A, Li P. Active-reactive optimal power flow in distribution networks with embedded generation and battery storage. IEEE T Power Syst 2012; 27: 2026–2035.

[14] Liang L, Zhong J. Optimal control of battery for grid-connected wind-storage system. In: IEEE 15th International Conference on Harmonics and Quality of Power; 17–20 June 2012; Hong Kong, China. New York, NY, USA: IEEE. pp. 701–706.

[15] Tewari S, Mohan N. Value of NAS energy storage toward integrating wind: Results from the wind to battery project. IEEE T Power Syst 2013; 28: 532–541.

[16] Wang J, Liu P, Hicks-Garner J, Sherman E, Soukiazian S, Verbrugge M, Tataria H, Musser J, Finamore P. Cycle-life model for graphite-$LiFePO_4$ cells. J Power Sources 2011; 196: 3942–3948.

[17] Agarwal V, Uthaichana K, DeCarlo RA, Tsoukalas LH. Development and validation of a battery model useful for discharging and charging power control and lifetime estimation. IEEE T Energy Conver 2010; 25: 821–835.

[18] Tran D, Khambadkone AM. Energy management for lifetime extension of energy storage system in micro-grid applications. IEEE T Smart Grid 2013; 4: 1289–1296.

[19] Ecker M, Gerschler JB, Vogel J, Käbitz S, Hust F, Dechent P, Sauer DU. Development of a lifetime prediction model for lithium-ion batteries based on extended accelerated aging test data. J Power Sources 2012; 215: 248–257.

[20] Ye Y, Shi Y, Tay AAO. Electro-thermal cycle life model for lithium iron phosphate battery. J Power Sources 2012, 217: 509–518.

[21] Zackrisson M, Avellán L, Orlenius J. Life cycle assessment of lithium-ion batteries for plug-in hybrid electric vehicles - critical issues. J Clean Prod 2010; 18: 1519–1529.

[22] Zamani AALI, Bijami E, Sheikholeslam F, Jafrasteh B. Optimal fuzzy load frequency controller with simultaneous auto-tuned membership functions and fuzzy control rules. Turk J Electr Eng Co 2012, 22: 66–86.